INTERFACE

rsif.royalsocietypublishing.org

Research

Cite this article: Sellés de Lucas V, Dutel H, Evans SE, Gröning F, Sharp AC, Watson PJ, Fagan MJ. 2018 An assessment of the role of the falx cerebri and tentorium cerebelli in the cranium of the cat (*Felis silvestris catus*). *J. R. Soc. Interface* **15**: 20180278.
http://dx.doi.org/10.1098/rsif.2018.0278

Received: 23 April 2018
Accepted: 2 October 2018

Subject Category:
Life Sciences–Engineering interface

Subject Areas:
biomechanics

Keywords:
finite-element analysis, biomechanics, carnivora, dura mater, falx cerebri, tentorium cerebelli

Author for correspondence:
Víctor Sellés de Lucas
e-mail: v.selles-de-lucas@2015.hull.ac.uk

Electronic supplementary material is available online at https://dx.doi.org/10.6084/m9.figshare.c.4260701.

THE ROYAL SOCIETY PUBLISHING

An assessment of the role of the falx cerebri and tentorium cerebelli in the cranium of the cat (*Felis silvestris catus*)

Víctor Sellés de Lucas[1], Hugo Dutel[1], Susan E. Evans[2], Flora Gröning[3], Alana C. Sharp[2], Peter J. Watson[1] and Michael J. Fagan[1]

[1]School of Engineering and Computer Science, Medical and Biological Engineering Research Group, University of Hull, Hull HU6 7RX, UK
[2]Department of Cell and Developmental Biology, University College London, London WCIE 6BT, UK
[3]School of Medicine, Medical Sciences and Nutrition, University of Aberdeen, Aberdeen AB25 2ZD, UK

VSdL, 0000-0003-0814-516X; ACS, 0000-0001-5117-5335

The falx cerebri and the tentorium cerebelli are two projections of the dura mater in the cranial cavity which ossify to varying degrees in some mammalian species. The idea that the ossification of these structures may be necessary to support the loads arising during feeding has been proposed and dismissed in the past, but never tested quantitatively. To address this, a biomechanical model of a domestic cat (*Felis silvestris catus*) skull was created and the material properties of the falx and tentorium were varied for a series of loading regimes incorporating the main masticatory and neck muscles during biting. Under these loading conditions, ossification of the falx cerebri does not have a significant impact on the stress in the cranial bones. In the case of the tentorium, however, a localized increase in stress was observed in the parietal and temporal bones, including the tympanic bulla, when a non-ossified tentorium was modelled. These effects were consistent across the different analyses, irrespective of loading regime. The results suggest that ossification of the tentorium cerebelli may play a minor role during feeding activities by decreasing the stress in the back of the skull.

1. Introduction

The dura mater is a fibrous membrane that covers the brain and spinal cord. It further extends into the cranial cavity in the shape of four folds or projections, two of which are the falx cerebri and the tentorium cerebelli. The falx cerebri divides the two cerebral hemispheres, while the tentorium separates the cerebral lobes from the underlying cerebellum (figure 1). Both the falx and tentorium are commonly found across a variety of mammal species, albeit not necessarily with the same degree of development [1]. Moreover, some species exhibit an ossified falx or an ossified tentorium; occasionally both. Ossification can also be a prenatal or a postnatal process, and these differences in developmental patterns led Nojima [2] to discriminate between the prenatal carnivore type (e.g. Marsupialia, Sirenia, Carnivora) and the postnatal dolphin type (some Cetacea and Primates). The degree of tentorial ossification also varies across species. In carnivorans, the level of ossification ranges from none in the striped skunk (*Mephitis mephitis*), to partial (Canidae), or complete, as in members of the Felidae [3].

The functional role of the ossification of these structures remains unclear. Nojima [3] dismissed the idea that an ossified tentorium aids in the protection of the carnivoran brain during locomotion and feeding. This argument is largely based on the evidence that other animal groups which perform similar activities, such as most herbivores and rodents, do not exhibit ossification. However, this is found on casual observation, and to date no specific analysis has been performed to support or reject it. In this study, we examine quantitatively the biomechanical role that the falx and the tentorium play in the

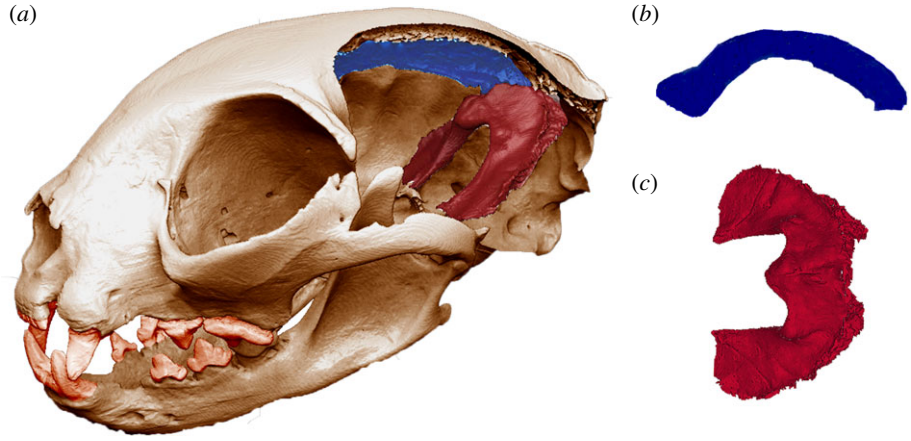

Figure 1. (*a*) The skull used for the *in silico* model after performing a virtual parasagittal cut in the braincase to reveal the falx cerebri and the tentorium cerebelli (displayed in blue and red, respectively). (*b*) Falx cerebri in medial–lateral view. (*c*) Tentorium cerebelli in dorsal view. (Online version in colour.)

mammalian skull, and any particular effects for Carnivora that the ossification may offer under different biting regimes. To achieve this, we developed a detailed finite-element (FE) model of a domestic cat (*Felis silvestris catus*) skull which included the falx and tentorium.

Felis silvestris is a polytypic species that includes various different subspecies which can produce viable offspring when crossed, *F. silvestris catus*, the domestic cat, being one of them [4]. The use of this particular species has two main advantages: it is widely available for study and, being a felid, it has a fully ossified tentorium, in contrast to other carnivorans. Over the last 20 Myr, felids have maintained a similar body plan [5], a factor that has made this group especially popular for allometric studies [6]. Following this general trend, the ossified tentorium of the domestic cat's skull is also very similar to those of other felids. Moreover, it has been observed that in newborn cats the tentorium is in an almost complete stage of ossification [3].

2. Material and methods

The head of an adult *F. silvestris catus* specimen, obtained from a deceased animal donated to the Liverpool Institute of Veterinary Science for teaching and research, was scanned in an X-Tek HMX 160 microCT (μ-CT) system at the University of Hull, UK (scan resolution 61.7 μm in all three axes). The sex of the specimen is unknown, as the body was not used in this study. The stack of .TIFF images obtained from μ-CT scanning was then imported into Avizo (v. 9.0.1, Visualization Science Group) where segmentation of the different structures was achieved using a semi-automatic method, combining algorithms with further manual refinements. The skull was intact, apart from the cusp of the left canine tooth which was reconstructed digitally, while the first left premolar was also absent (no action was taken in this case, as it did not play any relevant role in the analyses). The mandible was also segmented in order to reconstruct jaw-closing muscle orientations. The nasal turbinates were represented independently and identified as a different structure, as was the nasal septum. Where possible, the delicate structures that compose the cribriform plate and the ethmoturbinates were maintained. The trabecular bone was visible in the CT scans and individual trabeculae were segmented. Voids in the trabecular bone and the empty spaces between the nasal turbinates were filled with a general filling material to simulate the presence of generic soft tissues, which also prevented errors during the FE solution arising from disconnected fragments of trabeculae. The cranial cavity was also filled with another material to reconstruct the gross volume of the brain and to allow modelling of the dura mater covering its surface at a later stage. However, as no other intermediate layers were modelled, this endocast should be regarded as a simplification of the brain, because it was connected directly to the bone in the model, and therefore the endocast surface strains are likely to be oversensitive to changes in bone strain. This prevents a more detailed analysis of the effects that the ossified structures might pose on this particular structure. The periodontal ligament (PDL) was included by covering the tooth roots and their proximal surfaces with a three to four voxel-wide layer of tissue (0.19–0.27 mm [7]). Although the ossified tentorium forms a continuum with the parietal bone, it was carefully segmented as an independent structure (from where it attaches to the internal parietal wall) in order to allow testing with different material properties during the analyses.

The falx cerebri was partially visible in the CT scans, being partly ossified in its posterior region, allowing it to be reconstructed. Although the ossification was unexpected in this species, it may not be such a rare occurrence, because a second dissected specimen (also donated to the Liverpool Veterinary School for teaching and research) exhibited what seemed to be similar patches of ossification (figure 2; although we did not carry out further analyses to confirm their precise composition).

After segmentation, an FE mesh was created, resulting in a model with nearly 5.9 million high-order (quadratic) tetrahedral elements. Avizo landmark tools were used to define the origin and insertion areas of the muscles, with the data required for this step gathered during the dissection of two specimen heads. The left side of the modelled specimen was dissected together with the second head. Dissection data were also supported with information gathered from Hartstone-Rose *et al.* [8], Laison *et al.* [9] and Turnbull [10]. The mass of each individual muscle was measured to allow calculation of its physiological cross-sectional area (PCSA). The relative sizes of the muscles of the two specimens and those values reported in the literature were consistent, although interestingly the whole muscle mass of the second specimen was 2.5 times greater, thus potentially 36% larger in each direction. (Note the pterygoid group was damaged in the second specimen, hence its weight was approximated by multiplying the value of the scanned specimen by the scaling factor of 2.5.) (See electronic supplementary material, table S1.)

The muscles were placed in a 10% formaldehyde solution and stored in a fridge for one month, at which time the muscles were digested in a 30% nitric acid solution for 72 h in order to separate the individual muscle fibres. The acid was then substituted with a 50% aqueous glycerol solution to stop the

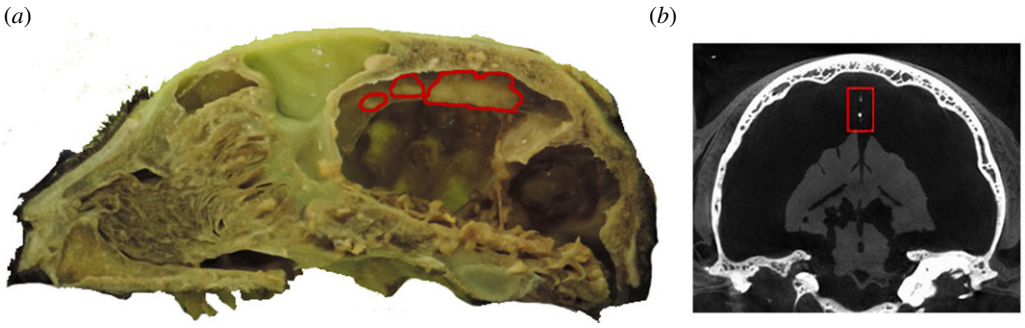

Figure 2. (*a*) Parasagittal cut of the second specimen, with patches of ossification (highlighted in red) in the posterior falx. (*b*) Coronal view of a CT image slice which shows an oval shape following the midline. (Online version in colour.)

digestion process. Ten to 15 random fibres for each muscle were isolated, photographed and subsequently measured with the software ImageJ [11] to estimate mean fibre length. The PCSA was calculated using the following formula [12]:

$$\text{PCSA} = \frac{\text{muscle mass (g)}}{\text{density (g cm}^{-3}) \times \text{fibre length (cm)}}.$$

The muscle density was estimated as 1.0564 g cm^{-3}, a value taken from Murphy & Beardsley [12] for the cat soleus, which has also been used in the studies of cat neck muscles [13] and felid masticatory analysis [8]. Different values have been reported for the intrinsic muscle tension (strength) produced by mammalian skeletal muscle, which typically ranges from 10 to 50 N cm^{-2}. An intermediate value of 30 N cm^{-2} was chosen from a feline bite force estimation study by Hartstone-Rose *et al*. [8]. Muscle force was calculated for the scanned specimen using the following formula:

$$\text{muscle force} = \text{PCSA (cm}^2) \times \text{tension per unit CSA (N cm}^{-2}).$$

Detailed PCSA values and muscle forces for the specimens are available as part of the electronic supplementary material, tables S2 and S3).

For the muscle insertion positions, the mandible was positioned at a gape angle of approximately 0°, i.e. complete occlusion. Because the specimen's head was not completely symmetric, landmarks were manually placed on both sides of the skulls, left and right side (instead of mirroring them) in order to maximize accuracy. A variable number of landmarks, between two and 16, were used for each muscle depending on its size. After calculating the x, y, z components of each force, a bespoke routine coded in R (v. 3.3.3 [14]) was employed to format the spatial information into ANSYS commands (Mechanical APDL, 14.5.7, ANSYS Inc., Canonsburg, PA, USA).

The dura mater was simulated in ANSYS by selecting all the surface elements of the brain endocast material and creating a covering layer of thin shell elements (ANSYS SHELL181). Shell elements are a simple but effective way to model very thin structures such as the dura, and the ability to modify section data was also useful for assigning different thicknesses to the structure during sensitivity tests. Although the dura actually extends over the brain and around the spinal cord, only the part that enclosed the brain was considered in this model, hence the dura was discontinued after reaching the infratentorial region.

Muscle wrapping was considered necessary for the superficial temporalis, given the origin area of the muscle and the curvature of the parietal and the temporal bones in the cat cranium. For this, we created a semi-automatic procedure in ANSYS to handle a muscle lying over a curvilinear surface. The process involves the creation of a series of paths, each consisting of a line of short 'hairs', using truss-type elements (ANSYS LINK180) positioned perpendicular to the bone surface (electronic supplementary material, figure S1). Landmarks for each individual hair were defined manually in Avizo and later imported into ANSYS. The node at the outer end of each hair was then connected to its neighbours with further link elements, thereby creating muscle strands wrapping around the cranium. The total force specified for the superficial temporalis muscle was then divided by the number of strands, and the resulting force was applied to the most inferior node of each strand.

The action of the neck muscles was also included in the model in order to simulate pull back and lateral pull. Neck muscle data were not available for the specimens considered in this study, hence the information was extracted from Reighard & Jennings [15], Wickland *et al*. [13] and Sebastiani & Fishbeck [16] (see electronic supplementary material, table S4). The *rectus capitis* group, which is composed of three individual muscles (*major, medius* and *minor*) was considered as a single unit for the analyses, while the *obliquus capitis caudalis*, with its origin on the atlas vertebra (C1), was not modelled. The number of landmarks per muscle, used to define the number of strands, was based on the size of the neck origin areas. As the original vertebrae and scapula were not present in the specimen, two octagons with different sizes were modelled and imported into Avizo to provide a surface for easier placement of the insertion landmarks. A small octagon was positioned at the axis vertebra (C2) and a larger one at the scapula, closely following the bone's orientation (electronic supplementary material, figures S2 and S3). The purpose of the octagonal shape was only to provide topological information (vertex and sides) to place the landmarks more easily. The neck muscle origin and insertion landmarks were then imported into ANSYS and muscle strands defined as flexible link elements with equivalent soft tissue material properties.

2.1. Material properties

The model was assigned bone material properties taken from the cortical bone of domestic dogs (Young Modulus, i.e. $E = 13.7$ GPa; $\nu = 0.30$), following Slater & Van Valkenburgh [6] in which these values were applied to various felid species. To the best of our knowledge, there are no material property data for the cat's dura in the literature, but human values are well known and were selected as a reasonable approximation ($E = 31.5$ MPa; $\nu = 0.45$ (after Kleiven & Holst [17])). The same applies to the PDL ($E = 50$ MPa; $\nu = 0.49$) which was taken from Rees and Jacobsen [18]. A 0.5 MPa value was assigned to the remaining generic soft tissues [19], including the brain endocast, link elements and filling materials ($\nu = 0.45$).

All material properties assigned to the different tissues were assumed to be isotropic, homogeneous and linear elastic, as it has been demonstrated that models using these properties still produce reasonable estimates of the stress and strain distributions [20–22]. Also, as this study focuses on a comparison of two versions of the same model by varying the material properties of the structures of interest, minor inaccuracies in the

Table 1. Sensitivity test values for the dura mater and other soft tissues (which also include the filling materials and the link elements).

sensitivity test	values tested	standard value used
Young's modulus (MPa) of dura mater	3, 31.5, 300	31.5 MPa[a]
thickness (mm) of dura mater	0.2, 0.55, 1.5	0.55 mm[b]
Young's modulus (MPa) of other soft tissues	0.5, 5, 50, 500	0.5 MPa[c]

[a]Kleiven & Holst [17].
[b]Cotton *et al.* [23]
[c]Huempfner-Hierl *et al.* [19].

material properties will not be critical as long as these remain constant in both versions. Nevertheless, because specific material property data for *F. silvestris catus* were not available, sensitivity tests were undertaken for the soft tissues, to assess their impact on the results (table 1). All these tests were performed for a bilateral canine bite. A dura mater thickness of 0.55 mm was taken from Cotton *et al*. [23] for humans, but further sensitivity tests with constant thickness values of 0.2 and 1.5 mm were also undertaken. The dura mater analyses were also carried out with values of 3 and 300 MPa, and for the generic facial soft tissue various values (5, 50 and 500 MPa) were tested independently. Sensitivity tests were also carried out to assess the importance of wrapping the superficial temporalis.

2.2. Boundary conditions

The skull was subjected to bilateral and unilateral canine and carnassial bites with different falx and tentorium material properties simulating either soft dural or hard osseous tissues in various combinations (see electronic supplementary material, table S5). For the bilateral canine analyses, one node was constrained dorsoventrally at the tip of each canine, with one node at the left glenoid fossa constrained in all degrees of freedom and the opposite node on the right side constrained in two directions (anteroposteriorly and dorsoventrally). These minimal constraints reduce the risk of artefacts from over-constraining the model [24,25]. For the unilateral canine analyses, only the node at the tip of the left canine was constrained. For the carnassial analyses, the same configuration at the glenoid fossae was maintained, but the anterior constraints were located at the notch between the paracone and the metacone of each carnassial (left carnassial in the case of the unilateral biting).

Additionally, two extrinsic loading regimes were applied to the model, one to simulate a pullback movement, the other a lateral pull. Similar types of analyses have been performed in previous studies of felids [6,26], but using different approaches. Here, the extrinsic loading conditions were applied in combination with biting by applying the muscle forces *and* reaction forces at the glenoid fossae and the canines for bilateral biting as predicted by the previous analyses. (In theory, these forces place the loaded skull in perfect equilibrium; however, due to unavoidable rounding errors in the software, there will inevitably be some, albeit negligible, out-of-balance force.) In addition, while the bite force loading was maintained, further loads were superimposed to simulate the pullback or lateral pull action, thereby replicating the loading of the skull *in vivo*. Two constraint conditions were applied: one with, and one without the neck. For the first model, without the neck, three locations on the posterior cranium were minimally constrained: two at the occipital condyles and the third located between them, over the foramen magnum. One node was constrained in all degrees of freedom, the second in only two directions (anteroposteriorly and dorsoventrally), while the third (over the foramen magnum) was constrained anteroposteriorly only. In the second variation, when the neck was modelled, all nodes corresponding to the muscle insertion points were constrained in all degrees of freedom. For the pullback simulation, once a bite force loading and the constraint option had been specified, an arbitrary pullback force of 25 N was applied to the upper posterior area of each canine, directed in a posterior–anterior direction, and subjecting the skull to tensional forces. For the lateral pull, the same force was applied to the left lateral surface of the canines. Thus, the two loading analyses were carried out with and without the neck structure, and the differences compared.

The total maximum bite force predicted by the model, measured at the tip of the canines for a bilateral bite, was 101.1 N, while the unilateral carnassial bite force was predicted to be 175.8 N. By using a modified version of the dry skull method [27], Sakamoto *et al.* [28] estimated a canine bite force of 177 N based on the skull width of 14 specimens of *F. silvestris catus* (median skull width, 62 mm; the skull width of our model is 75 mm, measured across the zygomatic arches, following Sakamoto & Ruta [29]). By contrast, using the same dry skull method, Christiansen & Wroe [30] (skull width not provided) reported a lower value of 73.3 N.

Performance of the skulls was evaluated by considering the von Mises stress value as this measure has been employed previously to assess skull behaviour (including earlier research in felid cranial biomechanics, such as McHenry *et al.* [31], Wroe [26] and Slater & Van Valkenburgh [6]). Von Mises stress is also convenient because it is a scalar function combining the three principal stresses, is related to the von Mises failure criterion, and is useful for comparing the performance of complex three-dimensional geometries.

Owing to the large number of comparative analyses performed in this study, difference plots are used to present the results in an easy and concise manner, and in such a way that even small differences in stress values become immediately evident (electronic supplementary material, figure S4), as it has been done in previous research [7]. For the difference plots, the following convention is used for all the results: the minuend of the subtraction is always the model with the osseous material properties while the subtrahend is the model with the soft tissue material properties. Thus negative values (cold colours) represent areas in which stress is lower in the osseous model, and positive values (warm colours) are areas in which stress is higher in the osseous model, and areas with no significant stress differences are centred around green. More even stress distributions and lower stress values represent a structure more adapted to withstand stresses under a particular loading regime [6].

2.3. Sensitivity tests

The preliminary sensitivity tests demonstrated that neither the stress magnitude nor distribution was significantly affected by the variations considered. As a result, detailed stress plots are not presented here, and the following summarizes the outcome of those investigations. Changes in dura mater thickness did

not lead to any discernable differences in the stress pattern and magnitude in the bone. Similarly, no meaningful differences were noted between dura mater elastic modulus values of 3 and 30 MPa, but there was a slight decrease in stress in the skull roof area for a value of 300 MPa, as would be expected. The sensitivity tests also demonstrated that using the higher elastic modulus value for the (soft tissue) cavity filling materials resulted in lower stresses across the skull, but the changes were negligible between 0.5 and 50 MPa. Concerning the muscle wrapping, and ignoring the local artefacts caused by the attachment of the muscle 'hairs' of each wrapping strand, again almost imperceptible variations in stress distribution were observed through the model. During bilateral canine biting, changes in bite force between the models with and without muscle wrapping, as measured at the tip of both canines, were also negligible (less than 1 N). Increasing the number of muscle strands would have distributed the loading more evenly over the bone, but it seems highly unlikely that it would have changed the overall conclusion of this test, as the direction of the resultant force would not change.

3. Results

After the sensitivity tests, the model was subjected to a series of intrinsic and extrinsic loading regimes in which canine and carnassial biting were simulated. Considering the models with a soft falx and an ossified tentorium first (i.e. the natural condition in *F. silvestris catus*), for the bilateral canine biting simulation stresses were equally high in the rostrum, the zygomatic arches and the palatine and presphenoid bones (electronic supplementary material, figure S5, left columns). In the rostrum, the nasal bones experience lower stresses than the surrounding bones, with the stress transmitted through the maxilla and into the frontal bone, until it reaches the approximate location of the coronal suture, where it dissipates. Regions of low or no stress can be identified within the parietal and interparietal bones, the tympanic bullae and the postorbital processes. In the carnassial bilateral biting simulation, stresses in the rostrum and the palatine were greatly reduced but remained constant in the zygomatic arches and seemed to be slightly higher throughout the orbit and in certain areas of the zygomatic bone. With unilateral biting, either with canine or carnassial teeth, stresses were higher on the working side in both the rostrum and the cranial roof (electronic supplementary material, figure S5, right columns). It is also worth noting that the stress at the back of the skull remains essentially unchanged for all these loading regimes. In the case of the extrinsic loads with an ossified tentorium, the pullback loading regime seemed to most closely replicate the simple bilateral bite (electronic supplementary material, figure S6). For the lateral pull, higher stresses manifested in the skull roof of the side opposite to the applied force. The largest differences between the two sides seemed to be located in the frontal bone and postorbital processes. Slight variations of stress magnitude were detected with the inclusion of the neck muscles in the analyses for either case, but there were no meaningful differences in stress distribution.

When models with ossified structures are compared to those with soft structures, differences in stress distribution and magnitude in cranial bone are also uncommon, regardless of the biting regime. Changes in the material properties of the falx cerebri do not lead to any discernible variations in the external skull stress patterns. However, difference plots demonstrate that the models with an ossified tentorium consistently exhibit lower stress values in the parietal and temporal bones, including the tympanic bulla (figures 3 and 4), with slight or minor differences depending on the particular regime. To provide further detail about the differences, 40 nodes at three sample locations of approximately 0.5 mm diameter were probed (electronic supplementary material, figure S7) for both ossified and non-ossified tentorium models during a bilateral canine biting regime. The highest stress decrease identified was 2.11 MPa at the inferior region of the temporal bone. Also, locally high stresses are observed in the interparietal and the sagittal crest for the lateral pull plus biting regime with no neck. These appear to be a consequence of the oversimplified constraints applied, causing the load path to be focused through those regions, because the equivalent version with neck muscles does not display them, and therefore they probably do not have mechanical significance. It is worth noting that stresses in the rostrum and the anterior area of the skull roof remained unaltered for all cases tested.

Examination of the stresses in the tentorium both ossified and non-ossified versions (figure 5 and electronic supplementary material, figure S8; note the different scales of the contour plots) shows that higher stresses are located anteriorly, with peak stress values in the area in contact with the parietal wall, and lower values in the borders of the tentorial notch. Apart from these differences in magnitude, the actual stress distribution remains unchanged for the different material properties and biting regimes. In the falx cerebri (figure 6), the stress is more unevenly distributed, but appears to be higher at the anterior third (especially in the soft falx cerebri) and the posterior end, particularly in the osseous falx for all regimes except the carnassial unilateral biting, and in the soft falx for both canine bites. The stresses in the osseous falx and tentorium are to various degrees of magnitude higher than those in the versions with soft tissue material properties, but in the extrinsic biting regimes (electronic supplementary material, figure S9) the soft falx seems to experience higher stresses overall. Moreover, adding or removing the dura mater layer over the brain endocast surface does not seem to have any effects on the results. In general, the cranial vault of the cat skull does not experience meaningful amounts of tension or compression (electronic supplementary material, figure S10), but the area of the temporal bone where the tentorium is located is subjected to compressive stresses. Compression is also visible in the tentorium cerebelli wings and in the posterior end of the midline, at the attachment of the falx cerebri.

4. Discussion and conclusion

Our aim was to test whether the presence of the osseous falx or tentorium played a significant role in reducing stress in the cranial bones under different biting regimes in *F. silvestris catus*. We observed that changing their material properties did lead to a considerable reduction of stress in the originally softer structures (figures 5 and 6 and electronic supplementary material, figures S8 and S9), but we did not observe the same effect in the cranial bone when considering the model as a whole.

In the case of the falx cerebri, the alteration of its material properties did not lead to any changes in the von Mises stress

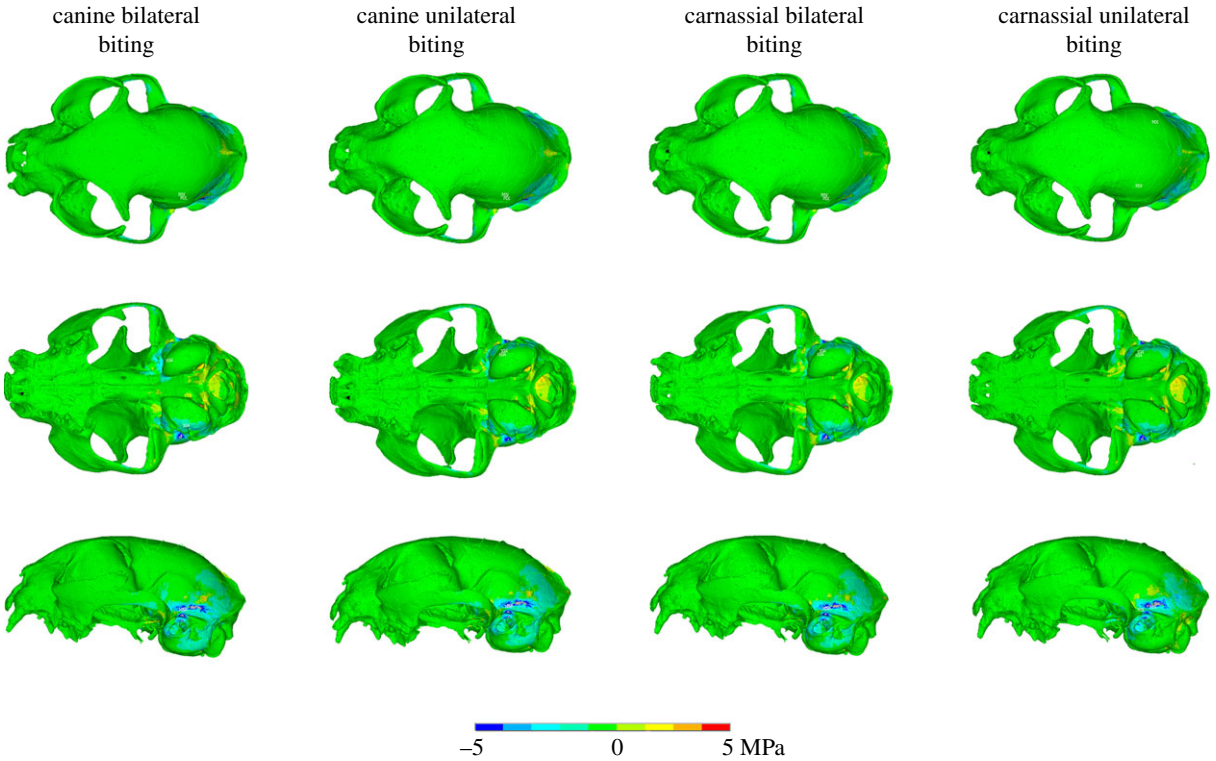

Figure 3. Von Mises stress difference plots for the (intrinsic) biting analyses, comparing osseous and soft tentorium models. (See electronic supplementary material, figure S4, for an explanation of the differencing process.)

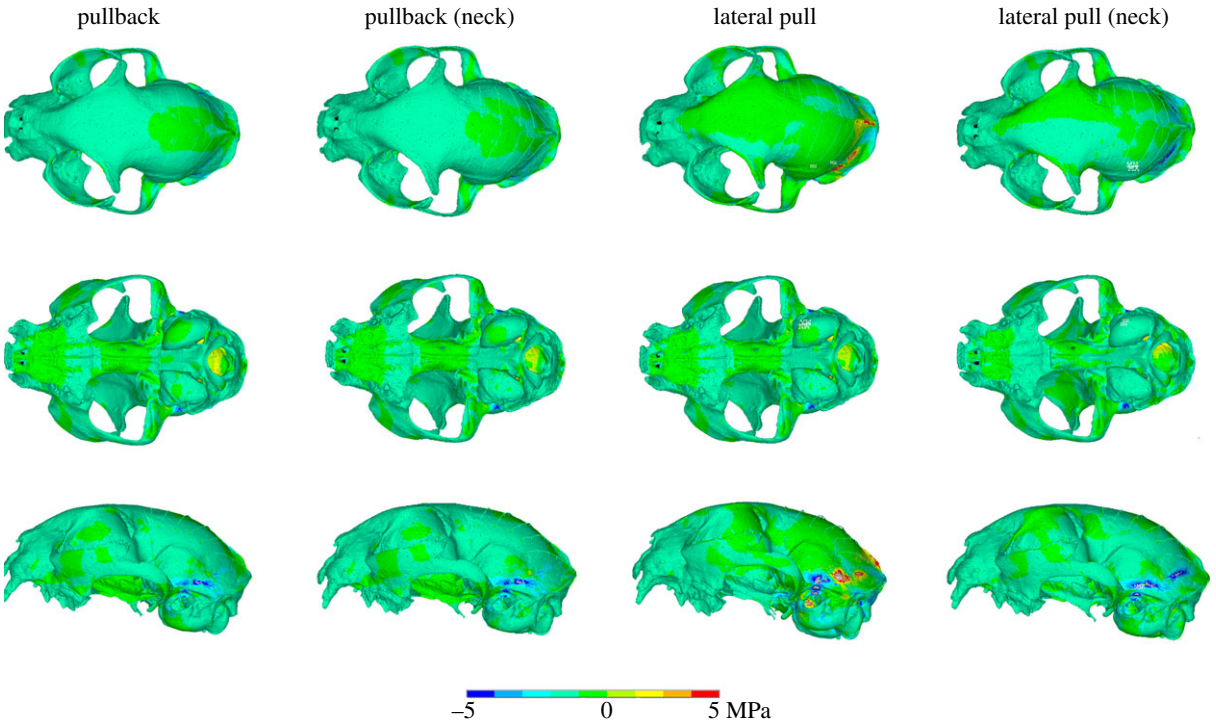

Figure 4. Von Mises stress difference plots for extrinsic analyses (biting plus pulling/tearing loads) comparing osseous and soft tentorium models. (See electronic supplementary material, figure S4, for an explanation of the differencing process.)

pattern of the cranium. According to the CT scans, the patches of ossification in the falx of the original specimen are mainly located in the middle to posterior end regions of the structure (in the case of the non-scanned specimen, ossification nodules appear in the middle section; figure 2). Thus, there does not seem to be any correlation between their location and the predicted stress pattern from the FE analyses (figure 6; electronic supplementary material, figure S9) and, in any case, it seems unlikely that these isolated nodules have any mechanical significance, because they appear disconnected from the cranial roof. For the tentorium cerebelli, the stress is concentrated at the end of both 'wings' of the structure (figure 5; electronic supplementary material, figure S8).

Stress differences between models with ossified and non-ossified tentoria were limited to the back of the skull, and

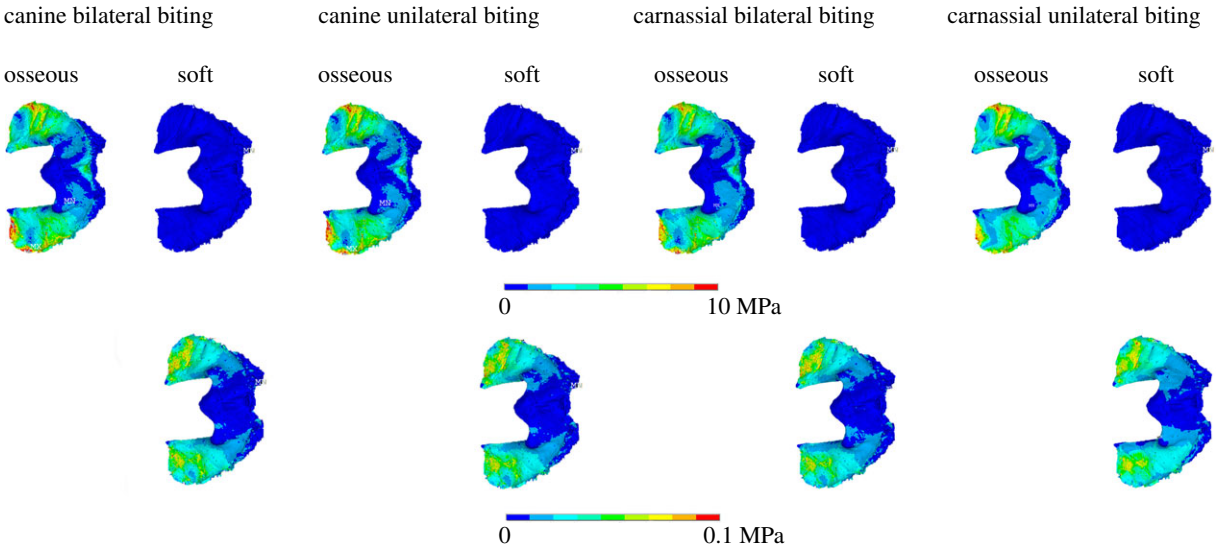

Figure 5. Von Mises stress plots for the tentorium cerebelli. Top row: osseous and soft tentorium in dorsal view for all intrinsic regimes. Bottom row: soft tentorium for the same loading regimes as the top row, but with adjusted contour levels to reveal the stress patterns.

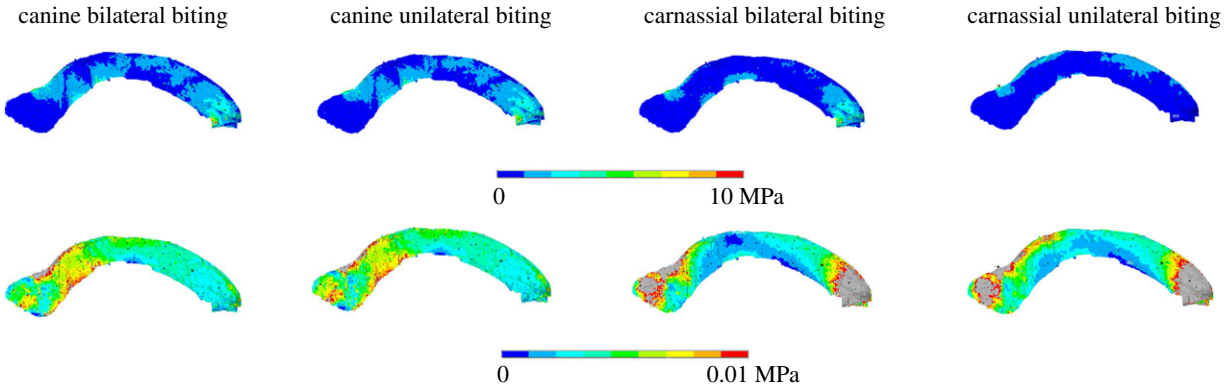

Figure 6. Von Mises stress plots for the falx cerebri. Top row: osseous falx cerebri in medial–lateral view for all intrinsic regimes. Bottom row: soft falx cerebri for the same analyses, but with adjusted contour levels to reveal the stress patterns.

specifically to the bones adjacent to the tentorium (parietal and temporal, including the tympanic bulla), and perhaps indicates that the tentorium may play a minor role during feeding. The difference in stress magnitude is, however, small (see the electronic supplementary material, figure S7) and therefore these results should be treated with caution. A more detailed model is necessary to assess the specific effects that this reduction in stress may pose on the brain. The area of interest at the back of the skull initially suggested a link between the neck muscles, as they are primarily attached to this region, but the extrinsic analyses that incorporated the neck did not reveal any meaningful differences. A recent study by McIntosh & Cox [32] demonstrates that, for mole-rats, a progressive increase in gape leads to a decrease in stress in the anterior regions of the cranium and an increase posteriorly. Felids are known to exhibit high values of maximum gape (61.3° in *Felis chaus* [33], a closely related species to *F. silvestris catus*), and it is possible that analyses with higher gape angles may reveal a more significant role for an ossified tentorium.

The use of simple linear elastic properties for the falx and the tentorium is one of the limitations of the current analysis. In particular for this study, the non-ossified materials are assumed to resist loads in both tension and compression, whereas in reality they are tension-only materials. As a result, the model may overestimate their influence. However, because the stiffness of these structures is orders of magnitude less than that of bone and their thicknesses are much smaller, their effect will be minimal, as demonstrated by the sensitivity studies. We believe therefore that this simplification does not alter the overall conclusions of the study.

Of the four different intrinsic biting regimes considered (electronic supplementary material, figure S5), the unilateral carnassial bite generates the highest peak stresses, being particularly high in the orbital region. From simple lever mechanics, it is evident that carnassial bites will generate higher forces than canine ones (e.g. 118.1 N versus 73.3 N, as calculated by Christiansen & Wroe [30]; 180.6 N versus 101.1 N in our model for the bilateral carnassial bite). The results from this study show that the most efficient biting regime in *F. silvestris catus* is the carnassial bilateral bite, as this is the one that generates the highest bite forces while experiencing the lowest overall stresses and the lowest peak stresses. In nature, biting and grasping are mostly carried out with the incisors and canines, while the carnassials are used for cutting and tearing food [34–36]. However, according to Orsini & Hennet [35], the upper jaw is larger than the lower in cats and therefore, for the teeth of both sides to be joined during mastication, the mandible has to be brought to one side, so it is highly doubtful that this type of carnassial

bilateral bite will ever be used in nature. Force variation between bilateral and unilateral carnassial bites (180.6 N versus 175.8 N) seems to be, in any case, negligible.

The skull shape of felids is rather conservative [37,38]. Some researchers have developed FE models of extinct saber-toothed cats and other felids [6,26,31,38] where biting regimes were based upon the cat's masticatory cycles and hunting behaviour. These studies demonstrated that felid skulls exhibit similar stress patterns when biting, and that stress is largely confined to the rostrum, the mandible and the zygomatic arch region. Our results follow a similar trend and replicate the ones obtained by Slater & Van Valkenburgh [6] from the cranium of *Felis lybica*, a closely related species, and also largely agree with the classic experimental study of a *F. silvestris catus* cranium performed by Buckland-Wright [34].

According to the literature, the most probable function for the tentorium cerebelli is to withstand the weight of the cerebral hemispheres [39,40], given that it is present in birds and mammals, and that both groups are characterized by a more developed brain than other tetrapods. Even when closely comparing different mammal species (see Klintworth [1], table 1), it seems reasonable to infer a relationship between tentorium development and encephalization quotient [41], using values of the tentorial index as indicators (the tentorium is considered to be more developed as the length of the straight sinus increases). The lower values are consistently present in orders with low brain quotients, such as Rodentia, Lagomorpha and Chiroptera, and increase in Carnivora, Cetacea and Primates [42]. The function of the falx cerebri may be to constrain the brain and limit displacement and rotation inside the cranium [43,44]. However, the presence of a bony falx and tentorium defies a simple explanation. The degree of ossification varies among different species and groups and it can develop before or after birth [1,3]. In carnivorans, an ossified tentorium cerebelli is present in almost all species, with the exception of *M. mephitis*. It is more developed in Felidae, Viverridae and Hyaenidae, where the structure is fully ossified and crosses the petrosa, than in other groups such as Phocidae or Canidae, where ossification does not reach the base of the skull [3]. An ossified falx is present in all pinnipeds, but also in the genus *Ursus* [3]. Sometimes, the condition manifests in species that normally exhibit a soft-tissue falx and tentorium: for example, partial falx ossification is relatively frequent in humans (around 10% of the adult population [45,46]) and tentorium ossification, while rarer, also exists [45,47].

In the analyses presented, all intrinsic and extrinsic biting regimes consistently resulted in the same pattern of stress across the cranium, which suggests that the function of the dural ossifications is not related to the forces exerted by struggling prey or in the action of pulling or tearing a carcass. However, feral *F. silvestris catus* mostly feed on small prey such as birds, mice and even some invertebrates [48]; therefore, similar tests should be run on larger predatory felids before completely ruling out a protective role for the dural ossifications during prey handling and feeding. This is especially important given the fact that small felids have proportionally larger braincases [49] and that may have a meaningful effect on the results. A new model with a more detailed brain would also help to resolve whether the stress reductions observed in the back of the skull lead to a corresponding decrease in the stress in the brain. Equally, it is important to note that the skulls of carnivorans in general, and felids in particular, are subjected to forces other than those associated with feeding, such as the ones resulting from acceleration or deceleration. In the past, various functional hypotheses have been proposed for the ossified falx and tentorium in carnivorans, notably that they serve as an extra protection for the brain to avoid injuries during locomotion (particularly relevant in the case of felids) or during mastication [3]. Nojima's argument to dismiss this is based on the fact that most carnivorans manifest ossification, but most herbivores do not, despite displaying a wide range of different speeds and behaviours. This still remains a strong case, but perhaps future research should focus on these and other alternative loading situations in order to address the role of the osseous falx and tentorium.

Ethics. The specimens of *F. silvestris catus* were obtained from deceased animals donated to the Institute of Veterinary Science, University of Liverpool, for teaching and research.

Data accessibility. Data supporting this work are available from the Dryad Digital Repository: http://dx.doi.org/10.5061/dryad.q33df2v [50].

Authors' contributions. M.J.F., S.E.E. and F.G. conceived the research programme and secured the funding. V.S.d.L. designed the study (with M.J.F. and S.E.E.) and created the models, undertook the analyses and drafted the paper. H.D. and V.S.d.L. undertook supporting experimental work, including specimen dissection (with S.E.E. and A.C.S.). P.J.W. and F.G. assisted in the FE modelling and analysis and interpretation of the results. All authors read and corrected earlier versions of the manuscript and approved the final version.

Competing interests. We have no competing interests.

Funding. We thank the Biotechnology and Biological Sciences Research Council (BBSRC) who provided funding for this research (BB/M008525/1; BB/M010287/1; BB/M008061/1).

Acknowledgements. The authors thank Sue Taft (University of Hull) for performing the μCT-scans, and the Institute of Veterinary Science and Nathan Jeffery (both University of Liverpool) for providing the specimens used in this study. The authors thank Phil Cox (University of York) and two other anonymous reviewers for their comments, insights and suggestions.

References

1. Klintworth GK. 1968 The comparative anatomy and phylogeny of the tentorium cerebelli. *Anat. Rec.* **160**, 635–641. (doi:10.1002/ar.1091600312)
2. Nojima T. 1988 Developmental pattern of the bony falx and bony tentorium of spotted dolphins (*Stenella attenuata*) and the relationship between degree of development and age. *Mar. Mamm. Sci.* **4**, 312–322.
3. Nojima T. 1990 A morphological consideration of the relationships of pinnipeds to other carnivorans based on the bony tentorium and bony falx. *Mar. Mamm. Sci.* **6**, 54–74. (doi:10.1111/j.1748-7692.1990.tb00226.x)
4. Driscoll CA *et al.* 2007 The Near Eastern origin of cat domestication. *Science* **317**, 519–523. (doi:10.1126/science.1139518)
5. Kitchener AC, Van Valkenburgh B, Yamaguchi N, Macdonald D, Loveridge A. 2010 Felid form and function. In *Biology and conservation of wild felids* (eds DW Macdonald, AJ Loveridge), pp. 83–106. Oxford, UK: Oxford University Press.
6. Slater G, Van Valkenburgh B. 2009 Allometry and performance: the evolution of skull form and function in felids. *J. Evol. Biol.* **22**,

2278–2287. (doi:10.1111/j.1420-9101.2009.01845.x)

7. McCormack SW, Witzel U, Watson PJ, Fagan MJ, Gröning F. 2017 Inclusion of periodontal ligament fibres in mandibular finite element models leads to an increase in alveolar bone strains. *PLoS ONE* **12**, e0188707. (doi:10.1371/journal.pone.0188707)
8. Hartstone-Rose A, Perry JM, Morrow CJ. 2012 Bite force estimation and the fiber architecture of felid masticatory muscles. *Anat. Rec.* **295**, 1336–1351. (doi:10.1002/ar.22518)
9. Laison F, Lautrou A, Azérad J, Pollin B, Lévy G. 2001 Superficial architecture of the jaw-closing muscles of the cat (*Felis catus*): the temporo-masseteric complex. *C. R l'Académie Sci. III* **324**, 855–862. (doi:10.1016/S0764-4469(01)01347-6)
10. Turnbull WD. 1970 Mammalian masticatory apparatus. *Fieldiana Geol.* **18**, 147–356.
11. Schneider CA, Rasband WS, Eliceiri KW. 2012 NIH Image to ImageJ: 25 years of image analysis. *Nat. Methods* **9**, 671. (doi:10.1038/nmeth.2089)
12. Murphy RA, Beardsley AC. 1974 Mechanical properties of the cat soleus muscle *in situ*. *Am. J. Physiol.* **227**, 1008–1013. (doi:10.1152/ajplegacy.1974.227.5.1008)
13. Wickland C, Baker J, Peterson B. 1991 Torque vectors of neck muscles in the cat. *Exp. Brain Res.* **84**, 649–659. (doi:10.1007/BF00230978)
14. R Development Core Team. 2008 *R: a language and environment for statistical computing*. Vienna, Austria: R Foundation for Statistical Computing. See http://www.R-project.org/.
15. Reighard JE, Jennings HS. 1901 *Anatomy of the cat*. New York, NY: Holt and Company.
16. Sebastiani A, Fishbeck DW 2005. *Mammalian anatomy: the cat*. Englewood, CO: Morton Publishing Company.
17. Kleiven S, von Holst H. 2002 Consequences of head size following trauma to the human head. *J. Biomech.* **35**, 153–160. (doi:10.1016/S0021-9290(01)00202-0)
18. Rees J, Jacobsen P. 1997 Elastic modulus of the periodontal ligament. *Biomaterials* **18**, 995–999. (doi:10.1016/S0142-9612(97)00021-5)
19. Huempfner-Hierl H, Bohne A, Schaller A, Wollny G, Hierl T. 2015 Does facial soft tissue protect against zygomatic fractures? Results of a finite element analysis. *Head Face Med.* **16**, 21-015-0078-5. (doi:10.1186/s13005-015-0078-5)
20. Strait DS, Wang Q, Dechow PC, Ross CF, Richmond BG, Spencer MA, Patel BA. 2005 Modeling elastic properties in finite-element analysis: how much precision is needed to produce an accurate model? *Anat. Rec.* **283**, 275–287. (doi:10.1002/ar.a.20172)
21. Bright JA, Rayfield EJ. 2011 The response of cranial biomechanical finite element models to variations in mesh density. *Anat. Rec.* **294**, 610–620. (doi:10.1002/ar.21358)
22. Gröning F, Bright JA, Fagan MJ, O'Higgins P. 2012 Improving the validation of finite element models with quantitative full-field strain comparisons. *J. Biomech.* **45**, 1498–1506. (doi:10.1016/j.jbiomech.2012.02.009)
23. Cotton R, Pearce CW, Young PG, Kota N, Leung A, Bagchi A, Qidwai SM. 2016 Development of a geometrically accurate and adaptable finite element head model for impact simulation: the Naval Research Laboratory–Simpleware Head Model. *Comput. Methods Biomech. Biomed. Engin.* **19**, 101–113. (doi:10.1080/10255842.2014.994118)
24. Dumont ER, Piccirillo J, Grosse IR. 2005 Finite-element analysis of biting behavior and bone stress in the facial skeletons of bats. *Anat. Rec. Part A* **283**, 319–330. (doi:10.1002/ar.a.20165)
25. Grosse IR, Dumont ER, Coletta C, Tolleson A. 2007 Techniques for modeling muscle-induced forces in finite element models of skeletal structures. *Anat. Rec.* **290**, 1069–1088. (doi:10.1002/ar.20568)
26. Wroe S. 2008 Cranial mechanics compared in extinct marsupial and extant African lions using a finite-element approach. *J. Zool.* **274**, 332–339. (doi:10.1111/j.1469-7998.2007.00389.x)
27. Thomason J. 1991 Cranial strength in relation to estimated biting forces in some mammals. *Can. J. Zool.* **69**, 2326–2333. (doi:10.1139/z91-327)
28. Sakamoto M, Lloyd G, Benton M. 2010 Phylogenetically structured variance in felid bite force: the role of phylogeny in the evolution of biting performance. *J. Evol. Biol.* **23**, 463–478. (doi:10.1111/j.1420-9101.2009.01922.x)
29. Sakamoto M, Ruta M. 2012 Convergence and divergence in the evolution of cat skulls: temporal and spatial patterns of morphological diversity. *PLoS ONE* **7**, e39752. (doi:10.1371/journal.pone.0039752)
30. Christiansen P, Wroe S. 2007 Bite forces and evolutionary adaptations to feeding ecology in carnivores. *Ecology* **88**, 347–358. (doi:10.1890/0012-9658(2007)88%5B347:BFAEAT%5D2.0.CO;2)
31. McHenry CR, Wroe S, Clausen PD, Moreno K, Cunningham E. 2007 Supermodeled sabercat, predatory behavior in *Smilodon fatalis* revealed by high-resolution 3D computer simulation. *Proc. Natl Acad. Sci. USA* **104**, 16 010–16 015. (doi:10.1073/pnas.0706086104)
32. McIntosh AF, Cox PG. 2016 The impact of gape on the performance of the skull in chisel-tooth digging and scratch digging mole-rats (Rodentia: Bathyergidae). *R. Soc. open sci.* **3**, 160568. (doi:10.1098/rsos.160568)
33. Christiansen P, Adolfssen JS. 2005 Bite forces, canine strength and skull allometry in carnivores (Mammalia, Carnivora). *J. Zool.* **266**, 133–151. (doi:10.1017/S0952836905006643)
34. Buckland-Wright J. 1978 Bone structure and the patterns of force transmission in the cat skull (*Felis catus*). *J. Morphol.* **155**, 35–61. (doi:10.1002/jmor.1051550104)
35. Orsini P, Hennet P. 1992 Anatomy of the mouth and teeth of the cat. *Vet. Clin. N. Am. Small Anim. Pract.* **22**, 1265–1277. (doi:10.1016/S0195-5616(92)50126-7)
36. Reiter AM, Soltero-Rivera MM. 2014 Applied feline oral anatomy and tooth extraction techniques: an illustrated guide. *J. Feline Med. Surg.* **16**, 900–913. (doi:10.1177/1098612X14552365)
37. Sicuro FL, Oliveira LFB. 2011 Skull morphology and functionality of extant Felidae (Mammalia: Carnivora): a phylogenetic and evolutionary perspective. *Zool. J. Linn. Soc.* **161**, 414–462. (doi:10.1111/j.1096-3642.2010.00636.x)
38. Chamoli U, Wroe S. 2011 Allometry in the distribution of material properties and geometry of the felid skull: why larger species may need to change and how they may achieve it. *J. Theor. Biol.* **283**, 217–226. (doi:10.1016/j.jtbi.2011.05.020)
39. Bull JW. 1969 Tentorium cerebelli. *Proc. R. Soc. Med.* **62**, 1301–1310.
40. Jeffery N. 2002 Differential regional brain growth and rotation of the prenatal human tentorium cerebelli. *J. Anat.* **200**, 135–144. (doi:10.1046/j.0021-8782.2001.00017.x)
41. Jerison H. 1973 *Evolution of the brain and intelligence*. New York: NY: Academic Press.
42. Boddy A, McGowen M, Sherwood C, Grossman L, Goodman M, Wildman D. 2012 Comparative analysis of encephalization in mammals reveals relaxed constraints on anthropoid primate and cetacean brain scaling. *J. Evol. Biol.* **25**, 981–994. (doi:10.1111/j.1420-9101.2012.02491.x)
43. Kumaresan S, Radhakrishnan S. 1996 Importance of partitioning membranes of the brain and the influence of the neck in head injury modelling. *Med. Biol. Eng. Comput.* **34**, 27–32. (doi:10.1007/BF02637019)
44. Snell RS. 2010 *Clinical neuroanatomy*. Philadelphia, PA: Lippincott Williams & Wilkins.
45. Tanaka Y, Takeuchi K. 1974 Dural calcification from the neurosurgical point of view. *Neurol. Med.* **14**(Suppl.), 5–10. (doi:10.2176/nmc.14pt1.SUPPLEMENT_5)
46. Debnath J, Satija L, George RA, Vaidya A, Sen D. 2009 Computed tomographic demonstration of unusual ossification of the falx cerebri: a case report. *Surg. Radiol. Anat.* **31**, 211–213. (doi:10.1007/s00276-008-0408-4)
47. Tubbs RS, Mortazavi MM, Miller J, Shoja MM, Loukas M, Cohen-Gadol AA. 2015 Ossification of the human tentorium cerebelli. *Biomed. Int.* **3**.
48. Bradshaw JW. 2006 The evolutionary basis for the feeding behavior of domestic dogs (*Canis familiaris*) and cats (*Felis catus*). *J. Nutr.* **136**, 1927S–1931S. (doi:10.1093/jn/136.7.1927S)
49. Christiansen P. 2008 Evolution of skull and mandible shape in cats (Carnivora: Felidae). *PLoS ONE* **3**, e2807. (doi:10.1371/journal.pone.0002807)
50. Sellés de Lucas V, Dutel H, Evans SE, Gröning F, Sharp AC, Watson PJ, Fagan MJ. 2018 Data from: An assessment of the role of the falx cerebri and tentorium cerebelli in the cranium of the cat (*Felis silvestris catus*). Dryad Digital Repository. (http://dx.doi.org/10.5061/dryad.q33df2v)